Alexandria Engineering Journal (2022) 61, 10463–10476

Alexandria University

Alexandria Engineering Journal

www.elsevier.com/locate/aej
www.sciencedirect.com

# Comparative assessment of four low voltage fault ride through techniques (LVFRT) for wind energy conversion systems (WECSs)

**James Tait** [a,*], **Shuren Wang** [a], **Khaled Ahmed** [a], **Grain Philip Adam** [b]

[a] *Department of Electronic and Electrical Engineering, University of Strathclyde, Glasgow G1 1XQ, U.K*
[b] *Department of Energy, NEOM, Tabuk 49643, Saudi Arabia*

Received 14 January 2022; revised 15 March 2022; accepted 1 April 2022

**KEYWORDS**

Low voltage fault ride through;
Wind energy conversion systems;
Energy storage systems;
Superconducting magnetic energy storage;
Supercapacitor energy storage

**Abstract** This paper presents a comparative assessment of four low voltage fault ride through (LVFRT) techniques that alleviate the effects of power imbalance during AC network faults for voltage source converter (VSC)-based wind energy conversion systems (WECSs). The techniques appraised include a software-based coordinated control (CC) technique, commercially available dumping resistor (DR) technique, and two energy storage techniques, namely, superconductive magnetic energy storage (SMES) and supercapacitor energy storage (SCES). The techniques presented are technically viable solutions for alleviating impacts of AC network faults on the WECS. The techniques have previously been assessed by performance-based metrics, whereas this paper aims to form a more comprehensive assessment by expanding the scope from the performance-based comparison to include economic considerations and practical limitations. Based on qualitative review of technically viable designs, this study presents quantitative substantiation with time-domain simulations of symmetrical and asymmetrical AC network faults. The comparative assessment is formulated based on assessing key performance metrics including grid code compliance, electrical and mechanical stress reduction, LVFRT response speed, hardware implementation, system efficiency and investment reduction. The assessment findings suggest that a performance-based study fails to highlight the potential financial and practical barriers that may exist regarding the implementation of the LVFRT solutions especially with energy storage-based techniques. However, the flexibility, benefits and increasing feasibility regarding energy storage systems may make them a preferred option for LVFRT of critical WECSs.



## 1. Introduction

Global carbon emission targets and socio-economic pressures have seen the rise in renewable energy sources connected to energy networks. One of the key technologies employed to

* Corresponding author.
E-mail addresses: james.g.tait@strath.ac.uk (J. Tait), shuren.wang@strath.ac.uk (S. Wang), khaled.ahmed@strath.ac.uk (K. Ahmed), grain.adam@neom.com (G.P. Adam).

This work was supported by the Engineering and Physical Science Research Council (EPSRC) under Grant EP/L015471/1.

https://doi.org/10.1016/j.aej.2022.04.003
1110-0168 © 2022 THE AUTHORS. Published by Elsevier BV on behalf of Faculty of Engineering, Alexandria University.

**Nomenclature**

| | |
|---|---|
| $A$ | Wind turbine blade swept area |
| $\beta$ | Wind turbine blade pitch |
| $C_{DC}$ | DC-link capacitor |
| $C_p$ | Wind turbine power coefficient |
| $C_{SCES}$ | Supercapacitor |
| $E_{LVFRT}$ | Calculated DC-link energy during AC grid fault |
| $F$ | Wind turbine generator viscous friction |
| $I_{DC\_fault}$ | DC current during AC network fault |
| $I_{DC\_SMES}$ | Rated superconductive magnetic energy storage current |
| $i_{dqg}$ | AC grid *dq*-axis current |
| $i_{dqs}$ | Wind generator *dq*-axis current |
| $i_g$ | AC grid current |
| $i_s$ | Wind generator stator AC current |
| $J$ | Wind turbine inertia |
| $\lambda$ | Wind turbine tip-speed ratio |
| $L_{dqs}$ | Wind turbine generator *dq*-axis inductance |
| $L_g$ | AC grid filter inductance |
| $L_{SCES}$ | Smoothing inductor for supercapacitor energy storage system |
| $L_{SMES}$ | Superconducting magnetic energy storage coil |
| $\Omega$ | Wind turbine rotor speed |
| $\omega_g$ | AC grid angular velocity |
| $\omega_r$ | Wind turbine rotor angular velocity |
| $p$ | Wind turbine generator pole pairs |
| $P_b$ | Base active power converter rating |
| $P_g$ | AC grid active power |
| $P_l$ | DC-link capacitor active power |
| $P_{in}$ | DC-link active power input |
| $P_m$ | Wind turbine mechanical power |
| $P_{out}$ | DC-link active power out |
| $P_s$ | Storage/dumping resistor power |
| $\Psi_r$ | Wind turbine generator flux linkage |
| $Q_g$ | AC grid reactive power |
| $R$ | Wind turbine blade radius |
| $R_{DR}$ | Dumping resistor |
| $\rho$ | Air density |
| $R_s$ | Wind turbine generator winding resistance |
| $S_b$ | Base apparent power converter rating |
| $\tau$ | DC-link capacitor time constant |
| $T_e$ | Wind turbine generator electrical torque |
| $\theta_g$ | AC grid phase angle |
| $\theta_s$ | Wind turbine generator phase angle |
| $t_{clear}$ | AC network fault clearance time |
| $T_m$ | Wind turbine generator mechanical torque |
| $t_{rec}$ | AC network fault recovery time |
| $u_w$ | Wind speed |
| $V_{DC}$ | DC-link voltage |
| $V_{DC\_rated}$ | Rated DC-link voltage |
| $v_{dqg}$ | AC grid *dq*-axis voltage |
| $v_{dqs}$ | Wind generator *dq*-axis voltage |
| $v_g$ | AC grid voltage |
| $v_{ret}$ | Resultant AC voltage, during network fault |
| $v_s$ | Wind turbine generator stator voltage |
| $V_{SCES\_initial}$ | Initial supercapacitor voltage |
| $V_{SCES\_rated}$ | Rated supercapacitor voltage |
| $v_{trig}$ | AC voltage, which triggers LVFRT operation |

reduce the carbon emissions related to electricity generation is the wind energy conversions systems (WECSs). In 1997, there was approximately 7 GW of installed wind capacity globally, in comparison to 744 GW in 2020 [1]. WECSs will continue to form an intrinsic part of the power system's progress to achieve global carbon emission targets [2]. The increased penetration and intermittent generation of WECSs have raised concerns over system security and stability [3], such as oscillation issues [4], and low short circuit ratios (SCRs) [5].

Among all challenges, AC system faults cause the most severe conditions, inflicting high levels of stress on WECSs and therefore should be addressed sufficiently. Low voltage fault ride through (LVFRT) requirements, set by grid codes, state that WECSs must remain galvanically connected and transiently stable during AC network faults, with defined periods of time and levels of voltage (for example, voltage level of 0 - 0.15 pu and duration of 140 ms – 200 ms in [6]). Additionally, WECSs are typically required to deliver reactive power to the network during fault and post-fault, to ensure operation security, aid in voltage restoration, and minimize risk of voltage collapse [4]. The amount of reactive power delivery varies between grid codes; however, it is typically stated that WECSs should deliver the maximum reactive power without compromising the converter limits [7]. Grid codes stipulate what the WECS must withstand; they do not offer instruction on how this is achieved, and it can be assured that strong grid assumptions are made.

As the achievable active power output of utility-scale WECS increases, which are currently available at 15 MW by Vestas [7], and at 14 MW with GE [8] and Siemens-Gamesa [9]; PMSG-based WECS technology is widely utilized. It can be ascertained from the industry offerings that PMSG is becoming the dominant technology for wind power delivery, with doubly fed induction generators (DFIGs) being offered at lower power output levels [10]. Also, the controllability of the PMSG equipped with fully-rated converters is improved [11]. Induction generators (IGs) are typically fixed speed generators and rely on a strong AC grid, and during network faults require reactive compensation due to the collapse of the stator voltage [12]. Although DFIGs have improved controllability over IGs, they are sensitive to unbalanced faults, where additional AC connected hardware is required to manage circulating rotor currents caused by the imbalance between rotor and stator magnetic flux [13] due to their synchronous coupling to AC network. As PMSGs are synchronously decoupled from the network by adopted voltage source converters (VSCs), PMSG-based WECSs do not inherently respond to AC network faults, thus allowing the system to maintain with normal operational limits (i.e., rotor speed and torque), and/or provide the required reactive current [14].

Importantly, the AC network voltage sags prevent the normal active power transfer from the generator to the network [15]. Without taking proper measures, this will result in sharp rise of the power converter DC-link capacitor voltage, which can initiate system shutdowns and inflict high levels of stress on the WECS devices [16]. Several techniques have been proposed in the literature to mitigate the negative effects on the WECS and comply with grid codes during network faults. Real power containment methods are employed to maintain or limit the power flow into the DC-link from the generator side converter during an AC fault to keep the DC-link voltage within operating range [6]. Blade pitch controllers have been proposed for reducing the rotor speed, thus power flow into the DC-link. However, the slow dynamics of pitch controllers prevent adequate power regulation within the millisecond time scales usually required [14]. Although the power converter's fast dynamics can block the power flow into the system, this practice inflicts mechanical stress on the PMSG through rapid de-loading [14,15]. There is potential for pitch controllers to participate in a coordinated scheme, however, this would be limited to prolonged faults or during fault recovery periods [15]. Pitch controllers coordinated with partially rated ESS are proposed; however, the PMSG stresses are still significant [17]. Also, auxiliary equipment can be employed to mitigate the negative effects on the WECS. Resistor-based energy dissipation is a common method, which allows power flow from the generator side converter to the DC-link and dumps the excess energy as heat to maintain the DC-link voltage within narrow and acceptable limits [14]. Resistor-based methods are attractive due to the effectiveness, robustness, and simplicity [18]. Works relating to enhancement of converter dynamic performance during LVFRT consider DR, highlighting the effectiveness in alleviation of faults [19]. However, utility scaled WECSs will require forced convection or liquid cooled systems involving auxiliary supplies, mechanical equipment, and additional maintenance [20], making heat dissipation management a key challenge considering the structure of the overall WECS. Conventional control systems such as optimum torque control (OTC) do not include any feedback from the AC network to the grid side converter, thus during an AC network fault disturbance the generator side converter continues to export pre-fault power into the DC link [21]. A software-based coordinated control method can be utilized to regulate power flow into the DC link from the generator side converter tubs negating additional hardware, thereby reducing converter size and weight. Ref. [22] suggests utilizing a feedback signal of the grid side voltage to the generator side control system, allowing the PMSG to reduce the power output during an ac network fault, with a similar scheme proposed in [23] for a two terminal VSC-HVDC. The aim is to maintain the DC-link operating within the limit by including a feedback signal into the inner current loop control reference signal of the generator side converter. Still, drawbacks of this technique when applied to a WECS employing VSC and PMSG are the mechanical strains imposed on the PMSG due to rotor speed acceleration and torque reduction and overvoltage on the stator terminals associated with rapid change of voltage across the PMSG inductance. A DC-link voltage reference is adopted to initiate the de-loading of the PMSG when the DC-link voltage breaches a setpoint limit [24], where the authors acknowledged this method will not alleviate the stresses to the mechanical system and the DC-link voltage can be maintained within acceptable limits. However, the conducted experiment only considers small scale WECS with high PMSG impedances effect.

To avoid energy dissipation during LVFRT and mitigate additional complex equipment connected to the DC terminals of the WECS, energy storage system (ESS) based methods have been proposed as attractive solutions for power smoothing to improve output power quality, smooth undesired transients and provide post-fault support, especially for weak AC grids where power oscillations occur [25]. Many variations of ESS have been considered in literature. For example, flywheel energy storage has been proposed at wind farm level, which provides excellent support by releasing power into the networks during deep voltage sags [26]. However, its high cost, large footprint and complicated implementation make this method limited to certain schemes [15]. Commonly, static ESS elements installable at converter level can be connected into the DC-link and be operated for LVFRT. By employing this method, WECSs can actively maintain the DC-link voltage during faults and have desirable grid code compliance. Battery energy storage systems (BESSs) have a lower self-discharge rate than that of other comparable storage systems [6], but present practical challenges for wind energy applications due to chemical elements [15]. Although the state of existing superconducting magnetic-based energy storage technologies still requires improvement, they are attracting more attention for practical implementation in bulk power systems where the high performance is expected during extreme cases such as system faults [27–29]. Supercapacitor-based energy storage systems have been seen as a promising alternative. Although self-discharge issues and high capital cost exist [30], supercapacitors have high power density in terms of both size and weight, which are particularly suitable for short-term high-power applications [31]. A detailed evaluation of four different LVFRT techniques at wind turbine level expanding on ref. [31], which is non-comprehensive, is presented in this paper.

The studied techniques are coordinated control (CC), dumping resistor (DR), superconductive magnetic energy storage (SMES), supercapacitor energy storage (SCES), where design considerations are presented. A WECS integrated with each of these four techniques is modelled and subsequently used to perform quantitative comparisons between several LVFRT techniques. Therefore, the operational performance of each method during symmetrical and asymmetrical AC faults is identified. With the consideration of practical implementation, a seven metrics-based evaluation framework is established, where the strengths and weaknesses of each technique are presented. Thus, the presented work's major contributions are as follows:

- Comparison of four active power containment techniques via simulation of the PMSG-based WECS complying to grid codes,
- Comparison of physical attributes between conventional and storage-based techniques,
- Sizing design and cost analysis on each of the techniques applied for LVFRT applications and
- A comprehensive assessment of the evaluated techniques as the potentially feasible LVFRT techniques.

The remainder of this paper is organized as follows: Section II introduces the basic configuration and modeling of

WECS, including operation analysis during LVFRT. Each LVFRT technique is presented in section III, including system design and operational features. Simulation-based evaluation of each technique on the system performance is given in section IV. Section V presents an analysis of the practical implementation elements. In section VI, a comprehensive assessment considering seven major aspects is provided, whereas the conclusions are summarized in Section VI.

## 2. Wind energy conversion system (WECS) configuration and modeling

This section presents the WECS used for the comprehensive assessment including time-domain simulations, implementation analysis, etc. Each stage of the system will be presented with operating principles and mathematical equations. The proposed WECS system and control structure will form the base model in which the LVFRT techniques detailed in section 3 will be implemented.

The overall system is illustrated in Fig. 1(a) with each stage of the studied WECS. The PMSG stator is connected to IGBT based generator side VSC, which is controlled by the generator side controller and the control is shown in Fig. 1(b). The DC output of the generator side converter VSC is connected to the DC-link with the power flow indicated by $P_{in}$. The ESS/DR block indicates the location where the DR, SMES or SCES will be interfaced, with charging/dissipation power represented by $P_s$. The DC-link capacitor is represented by $C_{DC}$ with power flow into the capacitor designated by $P_l$. The output power from the DC-link is designated by $P_{out}$, with the grid side converter control structure detailed in Fig. 1(c). The AC output of the grid side converter is connected to the PCC via power transformer.

The wind turbine aerodynamic model utilized is based on (1) to (4) [32], where $P_m$ is the mechanical output power from the turbine, $C_p$ represents the turbine power coefficient, $\lambda$ is the tip speed ratio, $\beta$ is the pitch angle, $\rho$ is the air density, $A$ is the swept area of the turbine, $u_w$ is the wind speed, $R$ is the blade radius, $\Omega$ denotes the rotor speed, and $C_{1\text{-}6}$ are turbine coefficients.

$$P_m = C_p(\lambda,\beta)\frac{\rho A}{2}{u_w}^3 \tag{1}$$

$$C_p(\lambda,\beta) = C_1\left(\frac{C_2}{\lambda_i} - C_3\beta - C_4\right)e^{\left(-\frac{C_5}{\lambda_i}\right)} + C_6\lambda_i \tag{2}$$

$$\frac{1}{\lambda_i} = \frac{1}{\lambda + 0.08\beta} - \frac{0.035}{\beta^3 + 1} \tag{3}$$

$$\lambda = \frac{R\Omega}{u_w} \tag{4}$$

The PMSG can be modelled by (5) to (8) [33], where the $d$-axis and $q$-axis stator voltages and stator currents are represented by $v_{ds}$, $v_{qs}$, $i_{ds}$ and $i_{qs}$, constants $R_s$, $L_d$ and $L_q$ represent the stator resistance and inductance of the $d$ and $q$ axis respectively, $T_m$ represents the mechanical torque, $T_e$ represents electrical torque, $p$ represents number of pole pairs; $\omega_r$ is the rotor speed, $J$ is the inertia, and $F$ is viscous rotor friction coefficient.

$$\frac{d}{dt}i_{ds} = \frac{1}{L_{ds}}v_{ds} - \frac{Rs}{L_{ds}}i_{ds} + \frac{L_{qs}}{L_{ds}}p\omega_r i_{qs} \tag{5}$$

$$\frac{d}{dt}i_{qs} = \frac{1}{L_{qs}}v_{qs} - \frac{Rs}{L_{qs}}i_q - \frac{L_d}{L_{qs}}p\omega_r i_{ds} - \frac{\psi_r p\omega_r}{L_{qs}} \tag{6}$$

$$T_e = 1.5p[\psi i_{qs} + (L_{ds} - L_{qs})i_{ds}i_{qs}] \tag{7}$$

$$\frac{d}{dt}\omega_r = \frac{1}{J}(T_e - F\omega_r - T_m) \tag{8}$$

### 2.1. Generator side converter

The generator side converter ensures the delivery of the optimized power from the wind turbine to the DC-link using a maximum point power tracking system [34]. During an AC network fault, the generator side converter will continue to allow power flow into its DC side, which is as per design of the OTC control structure. The major drawback to this method is that a power imbalance attributed to an ac network fault will result in continuous charging of the DC link capacitor ($C_{DC}$). Fig. 1(b) depicts the control scheme, which is based on (9) - (11) [35], where $v_s$ represents the generator stator voltage. The rotor speed reference $\omega_r$* is derived from a look-up table that uses representative wind speed from a typical wind power curve, and the $v_{dqs}$ values are calculated by the inner loop of the current controller of the converter.

$$\begin{cases} \vec{i}_s = i_{ds} + ji_{qs} = ji_{qs} \\ i_s = \sqrt{{i_{ds}}^2 + {i_{qs}}^2} = i_{qs} \end{cases}, \text{with} ids = 0 \tag{9}$$

$$T_e = 1.5p\psi_r i_s \tag{10}$$

$$v_s = \sqrt{(v_{ds})^2 + (v_{qs})^2} = \sqrt{(\omega_r L_q i_{qs})^2 + (\omega_r\psi_r)^2} \tag{11}$$

### 2.2. DC-link dynamics

The DC-link voltage is commonly regulated by the grid side converter [21]. As can be seen in Fig. 1(a), the AC network faults create a mismatch between the power flowing into the DC-link ($P_{in}$) and delivered into the AC grid ($P_{out}$) which may lead to overvoltage [14] due to excess energy. This causes extra stresses and potentially catastrophic failure to the power switches in the power electronic converter or the capacitor if not well managed [36]. The rate in which the overvoltage occurs is dependent on the mismatched power ($P_l$) and the size of the DC-link capacitance. For a two-level VSC, the equivalent capacitance ($C_{DC}$) can be calculated by (12), where $S_b$ is the converter rated apparent power, $V_{DC\_rated}$ is rated DC-link voltage and $\tau$ is a time constant, selected as 5 ms, which is deemed to have a small enough voltage ripple and is capable of handling small transients present in steady state operation [37].

$$C_{DC} = \frac{\tau S_b}{0.5V_{DC\_rated}^2} \tag{12}$$

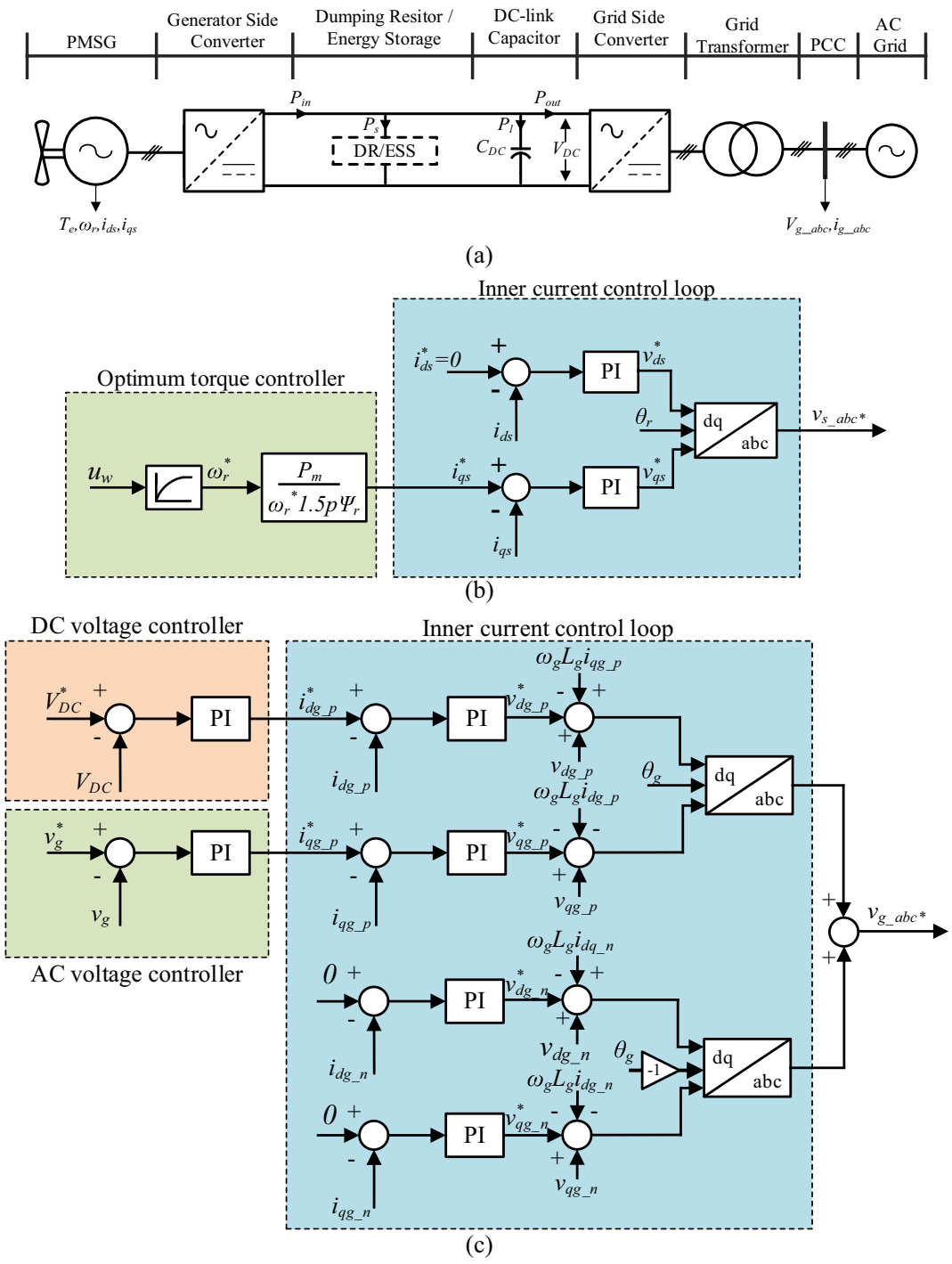


**Fig. 1** Grid connected WECS. (a) system configuration. (b) generator side converter control block diagram. (c) grid side converter control block diagram.

### *2.3. Grid side converter*

The grid side converter mainly aims to inject wind power into the AC network. The PI current controller typically operates in the synchronous reference (*d*-*q*) frame based in (13), and a double synchronous reference frame (DSRF) PLL is used for both positive and negative sequence current regulation [38], as shown in Fig. 1(c). The positive sequence controller is equipped with an outer loop which regulates the DC-link voltage ($V_{DC}$) and defines reference current of the *d*-axis inner current controller. Also, the outer loop of the *q*-axis facilitates an AC voltage ($v_g$) control and defines the reference of the *q*-axis inner current controller.

The WECS is required to ride through AC network faults, where detailed specifications are defined by each system operator (SO) (such as National Grid ESO [7], ENTSO-E [34], and IEEE [35]). If the system falls out of the stipulated profile, then

the generating unit is permitted to disconnect from the AC network [40]. The grid side converter plays an important role for such fault ride through, whereas the overall WECS must be under tight control to ensure safe operation.

$$\begin{cases} \frac{di_{dg}}{dt} = \frac{(v_{dg} - v_{di} + \omega_g L_g i_{qg})}{L_g} \\ \frac{di_{qg}}{dt} = \frac{(v_{qg} - v_{qi} - \omega_g L_g i_{dg})}{L_g} \end{cases} \tag{13}$$

### 2.4. Low voltage fault ride through (LVFRT) energy requirements for energy storage systems (ESSs)

ESS solutions are usually proposed for power smoothing or other long-term applications [41]. To utilize ESSs for LVFRT applications, it is imperative that the ESS employed has sufficient power and energy capacity, whereas the system specifications are usually given by the relevant SO and apply to all generating units.

In general, the parameters include a voltage threshold ($V_{trig}$), set to activate LVFRT measures; a recovery voltage ($V_{rec}$), which the generating unit must withstand for a longer-term period; and a retention voltage ($V_{ret}$) in which the generator must remain connected. The AC network fault clearance time ($t_{clear}$) specifies the time in which the ac network fault must be cleared in, and the system must withstand, on clearance of the fault the recovery time ($t_{rec}$). If the system parameters fall out with set parameters, then the generating unit is permitted to disconnect from the ac network. To ascertain the energy requirements ($E_{LVFRT}$) of ESSs during an AC fault, Eq. (14) can be used for basic ESS sizing [31].

$$E_{LVFRT} = P_b\left[\left(v_{trig} - v_{ret}\right)t_{clear} + 0.5(t_{rec} - t_{clear})\left(v_{trig} - v_{ret}\right)\right] \tag{14}$$

## 3. Four techniques for Low Voltage Fault Ride Through (LVFRT)wind energy conversion system (WECS) configuration and modeling

This section discusses four techniques for LVFRT to be integrated into a WECS system, which is akin to the system detailed in section 2 including basic design considerations and general technological characteristics.

### 3.1. Coordinated control (CC)

The technique proposed in [24] and [23] de-loads the PMSG by implementing a multiplication factor to the generator control reference ($i_q$). In [24] the multiplication factor is based on a look-up table which reduces based on the DC-link voltage with respect to setpoint. In [23] the de-loading factor is proportional to the AC network voltage magnitude. During an AC network fault, the system with CC de-loads the PMSG which may result in rotor speed increase and torque reduction, with the aim of containing DC-link voltage rise. This system negates hardware requirements, therefore is an attractive option. However, the key drawback is that the dynamics of the mechanical systems and the sudden change of voltage may cause overvoltage on the stator terminals along with rotor overspeed, which may not be fully highlighted by the small-scale machine-based experiment in [24].

### 3.2. Dumping resistor (DR)

Parallelly connected with the DC-link, the DR can provide protection to the DC-link capacitor from overvoltage and is commonly well coordinated with other LVFRT techniques. The DR can be implementation through a self-commutated semiconductor switch. Featuring relatively low hardware cost and control complexity (via hysteresis control or PI controller method), the DR method is easily implemented and widely used [14]. The significant drawbacks of the DR are the heat dissipation and wasted energy during the activation periods [11]. The DR must be sized at the full active power rating of the converter ($P_b$), where (15) provides a method to calculate the resistance, while $I_{DC\_fault}$ is the maximum allowable current of the resistor bank.

$$R_{DR} = \frac{P_b}{I^2_{DC\_fault}} \tag{15}$$

### 3.3. Superconducting magnetic energy storage (SMES)

The SMES can be implemented based on the circuit as shown in Fig. 2, where a two-quadrant chopper circuit facilitates bi-directional current capability of the SMES, with three modes of operation. Charging operation is achieved by operating both IGBT switches ($Q_1$ and $Q_2$). They are switched on allowing power flow into the SMES. Discharging mode of operation is achieved when both IGBT switches are in the off position permitting power flow via forward bias state of the diodes ($D_1$ and $D_2$). Stand-by mode of operation is achieved when only one of the IGBT's are on and the other is off (e.g. $Q_1 = 1$ and $Q_2 = 0$ or $Q_1 = 0$ and $Q_2 = 1$). During AC network faults, the excess energy in the DC-link can be stored in the SMES to provide superior response for the WECS. The coil inductance can be estimated based on (16) [29], where the $E_{LVFRT}$, calculated from (15) is the energy to be stored (in an extreme case based on the fault duration and excess power into the DC-link $P_l$), and $I_{DC\_SMES}$ is SMES rated current.

Superconductive material for energy storage has high efficiency, fast-responding speed, and high-power density [42]. However, major drawbacks of SMES are the high capital costs and operation requirements of cryogenic cooling, which incurs additional losses and requires specialist maintenance [28].

$$L_{SMES} = \frac{2E_{LVFRT}}{I^2_{DC\_SMES}} \tag{16}$$

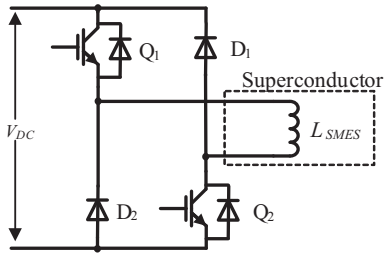


**Fig. 2** Schematic diagram of superconducting magnetic energy storage system

### 3.4. Supercapacitor energy storage (SCES)

Featuring high power density for low (ms) to medium (s) time scales [30], supercapacitors can be equipped in the DC-link and operated as energy storage in such LVFRT applications [43]. Fig. 3 shows the configuration with a bi-directional chopper interfacing the supercapacitor ($C_{SCES}$) and the DC-link. Ref. [31] provides guidance for sizing the supercapacitor based on the fault energy ($E_{LVFRT}$, calculated from (15)). Simply, assuming the allowable minimum and maximum supercapacitor voltages are 0.2 pu and 0.8 pu of the rated DC-link voltage respectively, with an initial charge voltage ($V_{DC\_initial}$) of 0.3 pu, the capacitance is estimated by (17). The design which considers initial charge voltage, internal resistance, current/power ratings, etc. is required, as articulated in [44].

Supercapacitors have generally high-power density, relatively long-life span, and low maintenance requirements in comparison to ESS such as batteries or SMES. However, the current drawbacks with SCES are the high capital costs (components and management systems) and self-discharge effect.

$$C_{sc} = \frac{2E_{LVFRT}}{\left(V_{SCES\_rated} - V_{SCES\_initial}\right)^2} \tag{17}$$

## 4. Simulation evaluation

This section details the WECS system from section 2 for the simulation study and presents the system performance with each LVFRT technique presented in section 3. System modelling is based on the parameters listed in Table 1, which defines the medium voltage collector network, line parameters, PMSG, the two-level back-to-back VSC, including grid side converter filters, etc. Two AC network fault cases, namely, three-phase to ground and single-phase to ground faults, are used to assess the LVFRT techniques. The wind speed is set to be 12 m/s, resulting in 1 pu torque and rotor speed ($\omega_r$). For the grid side converter, DC-link voltage reference ($V_{DC}$*) is set to be 1 pu and the reactive power reference ($v_g$*) is set to 1 pu, considering the grid support requirements [6]. Converter current limitation mechanism is adopted to limit the current amplitude to 1.2 pu.

In terms of the LVFRT performances to be investigated, four different configurations are simulated, namely, CC, DR, SMES, and SCES. For the DR, an IGBT switch is used to activate the energy dissipation and limit DC-link voltage; using a PI controller with the set-point being 1.2 pu of the DC-link voltage ($V_{DC}$). For the SMES, the modes of operation are defined by fixed set-points, where $1.05V_{DC}$ initiates charging and $0.95V_{DC}$ initiates discharging. For the SCES, the charging and discharging functions of the SCES circuit is configured in the same manner as the SMES, with an initial charge of 30%. The reason of the higher threshold for DR is to address issues of transients to reduce the power dissipation. This is not the case for energy storage-based methods such as SMES and SCES, as the stored energy can be fed back into the system.

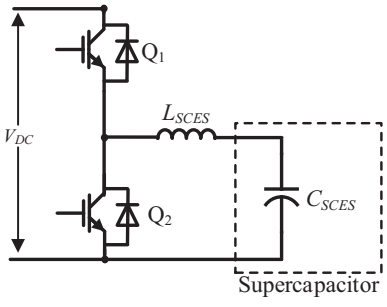


**Fig. 3** Schematic diagram of supercapacitor energy storage system

**Table 1** System parameters.

| Description | Value | Units |
|---|---|---|
| PCC voltage (ph-ph) | 25 | kV |
| Grid frequency | 50 | Hz |
| Grid short circuit ratio (SCR) | 10 | - |
| Transformer primary voltage (ph-ph) | 25 | kV |
| Transformer secondary voltage (ph-ph) | 0.69 | kV |
| Transformer resistance | 0.01 | pu |
| Transformer leakage | 0.2 | pu |
| Transformer power rating | 2.24 | MVA |
| PMSG mechanical power ($P_m$) | 2 | MW |
| PMSG torque ($T$) | 848.826 | kNm |
| PMSG rotor speed ($\omega_r$) | 2.36 | rad/s |
| PMSG stator resistance ($R_s$) | 0.82 | mΩ |
| PMSG $dq$-axis synchronous inductance ($L_{dq}$) | 1.57 | mH |
| PMSG rotor flux ($\psi$) | 5.8 | Wb |
| PMSG no. of pole pairs ($p$) | 26 | - |
| PMSG turbine inertia (J) | 50 | $Kgm^2$ |
| DC-link voltage ($V_{DC}$) | 1250 | V |
| DC-link capacitor ($C_{DC}$) | 2.5 | mF |
| Fault resistance | 1 | mΩ |
| Dumping resistor | 0.8 | Ω |
| SMES coil ($L_{SMES}$) | 0.45 | H |
| Supercapacitor ($C_{SCES}$) | 2.3 | F |
| Inner current controller PI gains | 1, 100 | - |
| Outer control loops PI gains | 1, 250 | - |

### 4.1. Symmetrical fault case

Fig. 4 shows the simulation results in a three-phase to ground fault at 0.3 s for a duration of 200 ms. Fig. 4(a-i)–(d-i) show the resultant AC voltage of 0 pu. Fig. 4(a-ii)–(d-ii) show the current waveforms during the fault, whereas Fig. 4(a-iii)–(d-iii) displays PCC active and reactive power. PMSG torque and rotor speed of each case are given in Fig. 4(iv) and (v) respectively. For the converter system, DC-link voltage, and powers (power flowing into the DC-link, $P_{in}$, power delivered into the grid side converter, $P_{out}$, and excess power absorbed by the DC-link device, $P_l$) are displayed in Fig. 4(vi) and (vii) respectively.

Fig. 4(a) shows that system with CC can suppress DC-link voltage rise and current oscillation to some extent. Although the generator side converter is restricting the power flow from the turbine into the DC-link, this still results in a DC-link voltage rise to about 1.6 pu, thereby still endangering the devices. The CC technique imposes mechanical stresses on the PMSG where the torque is reduced to 0 pu, resulting in an overspeed of around 1.6 pu and effectively blocking power flow to the DC-link, see Fig. 4(c-iv) and (c-v). The DR performs ade-

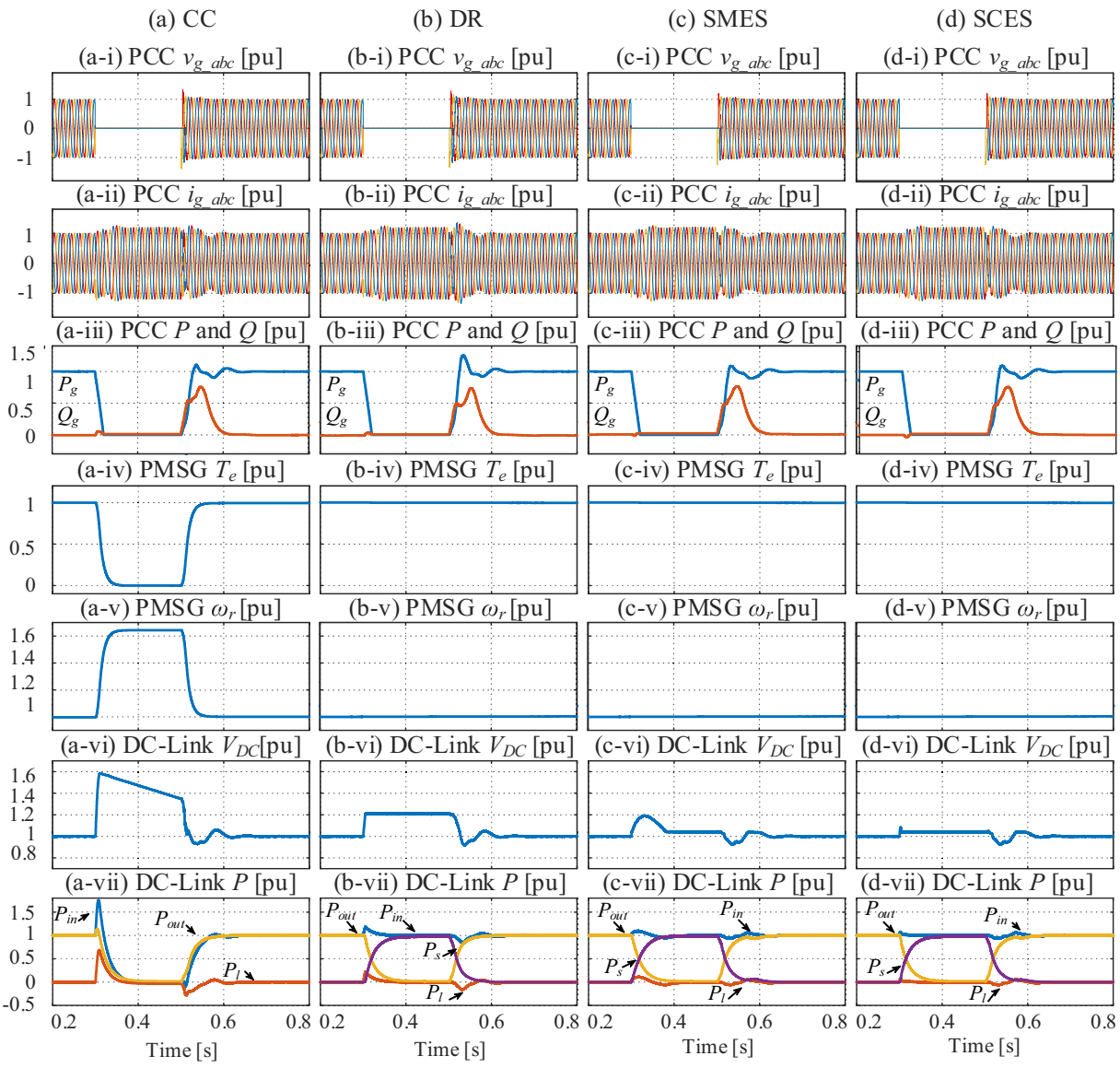


**Fig. 4** Simulation results of the system without and with four LVFRT techniques in the three-phase to ground fault case. (a) CC. (b) DR. (c) SMES. (d) SCES.

quately in comparison to the CC technique, with respect to containing the DC-link voltage within permissible limits, with the excessive power $P_l$ dissipated, see Fig. 4(d-iv), (d-v), and (d-vii). The WECS still has a minor overshoot of active power due to the sustained 1.2 pu DC-link voltage throughout the fault, as shown in Fig. 4(d-iii) and (d-vi). Both SMES and SCES can absorb the power, which cannot be injected into the AC grid, with DC-link voltage tightly controlled, see Fig. 4(c) and (d). The level of sustained DC-link voltage throughout the fault has a direct impact on the recovery time and overshoot of power. With regulated power flow during the fault, the post-fault power recovery for SMES and SCES is improved, see Fig. 4(c-ii) and (d-ii), where minimal overshoot can be observed compared to other methods. The main difference between SMES and SCES techniques is the minor DC-link voltage overshoot at the early stage of the fault on the SMES, which is mainly due to the coil dynamics (high inductance causes slow current changing rate), see Fig. 4(c-vi). The AC current of the grid side converter is limited with DR, SMES and SCES due to the normal DC-link voltage and converter operation, see Fig. 4(b-iii), (c-iii), and (d-iii).

Table 2 provides a numerical representation of key parameters of the WECS performance during the fault and recovery period, which forms a comparison to grid codes where applicable. The grid code selected is based on the most onerous values provided by ENTSO-E [39]. For each technique, the most onerous LVFRT of a fault that results in a 0 pu voltage fault for 200 ms has been adhered to consistently. The major difference between the techniques is the level of DC-voltage overshoot, with the highest case (CC) of 1.6 pu $V_{DC}$ rise. This is approximately 29% higher than those of the DR and SMES cases which is approximately 42% higher than that of the SCES. On initial activation the 1.2 pu overshoot of the SMES is characterized by the large inductance resulting with the observed overshoot characteristics which can be quantified and directly compared to [45]. Thus, SCES is the most capable

**Table 2** Performance results of three-phase to ground fault with comparison to grid code stipulations.

| Stage | Description | CC | DR | SMES | SCES | Grid Code |
|---|---|---|---|---|---|---|
| Fault | Min. 1ph-g grid voltage(pu) | 0 | 0 | 0 | 0 | 0 - 0.15 |
| Fault | Fault duration (ms) | 200 | 200 | 200 | 200 | 140 - 200 |
| Fault | Max. DC-link voltage (pu) | 1.6 | 1.2 | 1.2 | 1.05 | - |
| Recovery | PCC power overshoot (pu) | 1.2 | 1.3 | 1.1 | 1.1 | - |
| Recovery | PCC power recovery time (ms) | 150 | 100 | 120 | 120 | 500 |

of maintaining the DC-link voltage within tolerable limits. The DR results in the highest overshoot of active power to the AC network with $P_g$ reaching 1.3 pu, being approximately 8% higher than CC and approximately 17% higher than SMES and SCES. This shows that the ESS techniques result in the lowest overshoot during recovery. Although the recovery duration of the four techniques is within the grid code stipulation of 500 ms, CC has the longest recovery of 150 ms, making it 22% slower than the ESS techniques and 40% slower than the DR technique. For verification purposes, the DR performance has been compared to [14], the SMES performance has been compared to [45], and the SCES performance has been compared to [40].

### *4.2. Asymmetrical fault case*

Fig. 5 shows the simulation results with a single-phase to ground fault at 0.3 s for a duration of 200 ms. The presented waveforms and variables are the same as that of Fig. 4.

For the CC, the generator converter controller restricts power flow into the DC-link during the fault until the condition where average values of $P_{in}$ and $P_{out}$ are matched. Due to the slow dynamics of the PMSG, an initial overshoot of $P_{in}$ is present at the early stages of the fault, which results in an initial DC-link voltage rise of almost 1.3 pu before decaying before fault clearance, see Fig. 5(b-vi). In addition, there is a sustained overspeed of 1.2 pu, see Fig. 5(b-v), reducing the practical realization of this technique. This value is approaching the limit of the switching device rating and prolonged faults may result in damage to devices. The DR improves the performance by keeping the DC-link voltage within the 1.2 pu set-point, see Fig. 5(c-vi), however, this sustained level of DC-link voltage slightly affects the recovery of the system after fault clearance, resulting in a PCC active power overshoot of almost 1.1pu and slower recovery time than the other techniques presented, see Fig. 5(c-iii). Performance of the SMES and SCES, see Fig. 5(d) and (e) respectively, provide the most effective DC-link regulation out of the techniques presented with little distinguishable differences during such an asymmetrical fault. Also, the DC-link voltages are maintained at set-point, current regulation is correct and fast post-fault recovery is achieved.

Table 3 provides a numerical representation of key parameters of the WECS and converter system during the single-phase to ground fault and recovery period, which forms a comparison to grid codes where applicable. The most significant difference between the techniques is the level of DC-voltage overshoot with the highest case being CC where $V_{DC}$ rises to 1.3 pu. This is approximately 8% higher than the DR case and approximately 17% higher than the cases with ESS techniques. Also, the DR has the highest overshoot of active power to the AC network with $P_g$ reaching 1.2 pu, approximately 21% higher than the ESS options and approximately 26% higher than CC (negligible overshoot during the single-phase to ground fault recovery period). All the four techniques have approximately the same recovery duration, making them indistinguishable from each other.

## 5. Practical implementation consideration

Practical and commercial factors are key to the decision process of implementing such engineering techniques for LVFRT. This section analyzes the practical aspects of each of the LVFRT techniques. Taking the case listed in Table 1 as an example, an appraisal of practical and commercial implementation regarding the investigated LVFRT solutions can be presented considering major costs, size, weight, cooling method, efficiency, etc., as given in Table 4, except for CC due to the minimal cost and no physical properties.

### *5.1. DR*

The DR is designed based on a 2 MW dumping resistor bank such as that in [46]. Due to the heat dissipation of the resistor banks, the system requires forced convection cooling, with additional control supplies. The DR has many attractive features due to the low cost, volume, and weight. The importance of keeping cooling paths clear is stated in the manufacturer's instructions [46], showing heat management is a critical part of system. As stipulated in [46] it is imperative that the dissipated heat is managed correctly and malfunctions to the cooling system could result in failure to the DR, which in turn voids the grid code compliance of the WECS. The costs are estimated based on the suitably rated components including resistor banks [47,48] and IGBTs [49]. Importantly, among all the techniques, it is the most technically robust and commercially mature.

### *5.2. SMES*

The information on volume, weight, and cooling method of the SMES indicate high requirements on the engineering implementation, although this technique tends to have high round-trip efficiency [42]. Due to most systems being research-based, no clear information on the commercial aspects of SMES is readily available, whereas the information in [30,43] can be only used to ascertain a range of costs, which

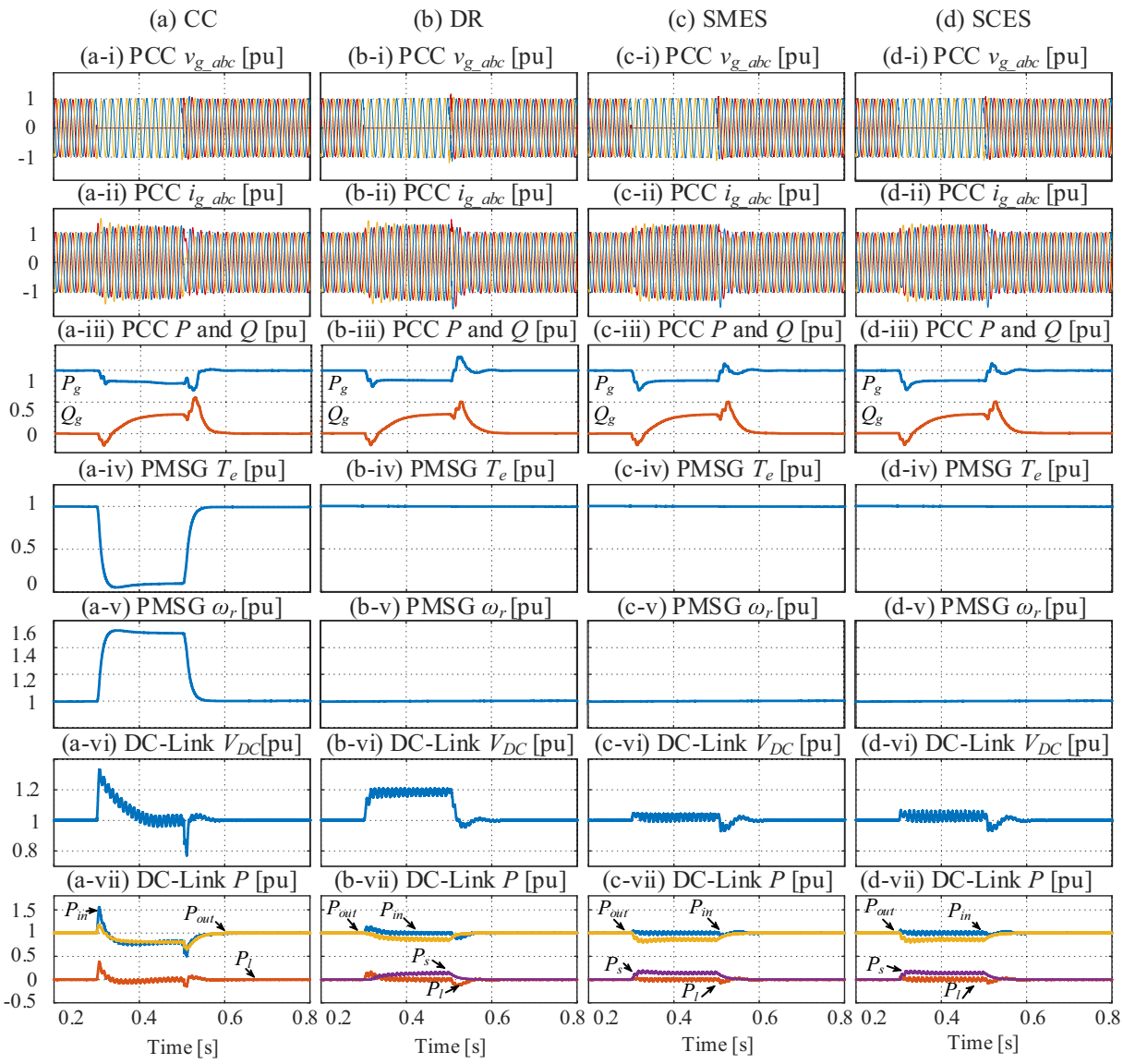


**Fig. 5** Simulation results of the system without and with four LVFRT techniques in the single-phase to ground fault case. (a) CC. (b) DR. (c) SMES. (d) SCES.

**Table 3** Performance results of single-phase to ground fault with comparison to grid code stipulations.

| Stage | Description | CC | DR | SMES | SCES | Grid Code |
|---|---|---|---|---|---|---|
| Fault | Min. 1ph-g grid voltage(pu) | 0 | 0 | 0 | 0 | 0 - 0.15 |
| Fault | Fault duration (ms) | 200 | 200 | 200 | 200 | 140 - 200 |
| Fault | Max. DC-link voltage (pu) | 1.3 | 1.2 | 1.05 | 1.05 | - |
| Recovery | PCC power overshoot (pu) | 1 | 1.2 | 1.05 | 1.05 | - |
| Recovery | PCC power restoration time (ms) | 50 | 50 | 50 | 50 | 500 |

is high and unsuitable for wind turbine level applications. Also, this technique requires the highest number of semiconductors. Practically speaking, the SMES could be deemed unviable for wind turbine level integration due to the physical complexities involved.

### 5.3. SCES

The engineering consideration of the SCES system can be estimated from design, which is sized based on [50] . The cooling requirement on the SCES system can be low, while the volume

**Table 4** Practical characteristics of the studied techniques.

| Considered items | DR | SMES | SCES |
|---|---|---|---|
| Volume [$m^3$] | 0.28 | 12 | 0.3 – 0.7 |
| Weight [kg] | 80 | 1,100 | 300 - 500 |
| Cooling method | Natural/forced convection | Cryogenic | Natural convection |
| Operation efficiency | N/A | 80% - 99% | 65% - 99% |
| Self-discharge percentage per day | N/A | 1% - 15% | 0.46% - 40% |
| Passive component cost [$] | 40k - 90k | 400k - 980k | 80k - 140k |
| Power electronics cost [$] | 1.5k | 3k | 3k |

and weight can result in difficult engineering constraint. The high levels of self-discharge and complexity of cell management system are also problematic. Currently, the cost of commercially available SCESs remain higher than DR [51], in addition to the DC/DC converter inductor [52]. With these factors taken into consideration, integration of SCES at wind turbine level might be practical with the cost expected to be reduced.

## 6. Comprehensive analysis

The key challenges during LVFRT of WECSs is to manage the active power that cannot be transferred into the faulty grid. Different techniques can be used to address that, but at the expense of imposing stresses at various points within the system. Fig. 6. presents the performance comparison of the four studied techniques with the designated metrics.

### 6.1. Grid code compliance

Grid codes do not provide specific values for the internal converter transient voltages and levels of fault voltages and current within the converter and state these must be based on converter capability, fault recovery limits including output power oscillations, and are permissible on recovery, providing they are adequately damped [7].

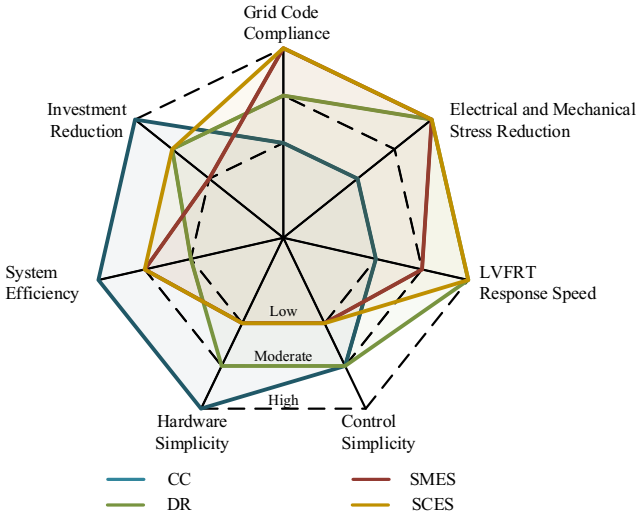


**Fig. 6** Performance comparison of the WECS with the presented techniques.

The highest level of DC-link voltage rise makes CC the least effective for grid code compliancy among the four assessed techniques, with DC-link voltage rise being approximately 29% higher than the DR and 44% higher than the ESS options; SMES and SCES. This is mainly due to the large DC-link voltage rise during the fault. A WECS with DR can meet the grid code stipulations and the resultant power quality is superior to that of CC, however, the recovery might result in overshoot in comparison to SMES and SCES for both symmetrical and asymmetrical faults. This overshoot and prolonged period are the result of the higher permitted operating point, set to avoid spurious operation during DC-link transients that may occur in normal cases. The overshoot of active power ($P_g$) for the DR is 8% higher than that of CC and 17% higher than that of the ESS techniques, with SMES and the SCES presenting a superior dynamic performance compared to the CC and DR methods. However, they have a marginally slower recovery period of 120 ms seconds in comparison to the DR. All techniques adhere to the 500ms recovery time stated by the grid codes.

### 6.2. Electrical and mechanical stress reduction

The electrical stresses using CC are the highest among all techniques, due to the highest level of DC-link voltage rise. The level of voltage rise would be at such a level where the electrical components would have exceeded their rated value and in the region where failure/shutdown occurs. In addition to the electrical components on the converter, the excess rotor speed may cause overvoltage on the stator terminals, causing stresses on the stator windings. The DR, SMES and SCES mitigate electrical stresses and keep the components within their permitted values. All techniques, with exception of CC, inflicted minimal stresses on the PMSG, via permitting uninterrupted power flow from the generator side converter to the DC-link. The CC de-loads the PMSG, which results in a level of torque rejection proportional to the AC network voltage, thereby resulting in rotor acceleration. This rapid de-loading characteristic results in a 100% difference to the torque and 60% of the rotor speed in comparison with DR, SMES and SCES. Although electrical machines have permitted levels of overspeed depending on the rotor construction, this level of overspeed would be considered to impose high levels of mechanical stress to the WECS and may initiate a generator shutdown.

### 6.3. LVFRT response speed

The CC response speed is the slowest of the techniques appraised due to the large time constants associated with the PMSG mechanical system and is difficult to improve by increasing the control loop bandwidth of the generator side control system, especially during severe faults. The DR has a fast LVFRT response; as soon as it is activated the power is dissipated. To contrast this, the charging of the large SMES coils results in slow dynamics when the fault is severe. The SCES has fast LVFRT response mainly due to the low time

constant of supercapacitors which results in a 1 ms settling time to setpoint in comparison with the SMES which takes about 80 ms. However, it should be noted that the response speeds are highly dependent on the system sizing.

### 6.4. Control simplicity

In general, implementing a feedback signal from the AC network voltage reference into the generator side controller torque calculation, the control for the CC, is simple. The DR also has a single PI controller with a reasonable set-point feeding a single IGBT switch. For LVFRT only and neglecting power smoothing functionality, the SMES has three operation modes, which need to be managed, as well as its energy storage (current) management. The same complexities apply to the SCES, where the system must balance the voltage across multiple cells in addition to ensuring charge and pre-charge levels are at an acceptable level to ensure optimum LVFRT performance. This makes the control systems for SMES and SCES complex.

### 6.5. Hardware simplicity

The CC is software based so effectively has no issues regarding hardware complexity. The DR's hardware scheme is dependent on the type of resistor selected and the cooling system design, which is essential for reliability and the longevity of the system. This is critical to the WECS. The SMES's complexities are attributed to its cryogenic cooling system, which requires specialist maintenance and highly sensitive components. The SCES is constructed of a high level of low voltage cells consisting of long series and parallel connected strings, which will all degrade at different rates depending on temperature and operating conditions.

### 6.6. System efficiency

The system with CC can be considered the most efficient due to no additional hardware involved. The DR by design is inefficient as all the energy captured is dissipated as heat. Theoretically, the SMES is highly efficient due to the low resistance of the superconducting material, however, self-discharging through power circuits and its own management system would affect the overall system efficiency. SMES may suffer from the power circuit internal resistance, and non-trivial levels of self-discharge.

### 6.7. Investment reduction

The system cost with CC cannot be evaluated on the same scale as the DR, SMES and SCES due to its lack of hardware. The DR is the lowest in cost of all the schemes. Although CC mitigates hardware costs, there may be additional costs from failure or maintenance due to the higher levels of mechanical stresses to the PMSG when compared to the other techniques. The DR, which is widely used in utility scale turbines, is the lowest cost device with SMES being a approximately 24 times higher at its widest price range The SMES costs, albeit the values are academic, are very high. The SCES has a large price scale, indicating an unattractive investment being a range of 12.5% cheaper than the DR to 250% more expensive, depending on the quality and type of supercapacitor selected. However, if the lower scale cost could be practically realized in the future, the SCES would be a candidate for turbine level performance enhancement.

### 6.8. Summary of assessment

Table 5 summarizes the four LVFRT techniques with focus on the main merits and demerits of each to form a direct comparison. The coordinated control (CC) has no hardware requirements, thus is the least expensive. However, uncertainty over the effect of PMSG longevity exists as there is no empirical evidence available to quantify the effects such stresses may have. This factor poses risk as may lead to high levels of operational expenditure. The electrical stresses CC imposes, chiefly through DC-link voltage rise, could be alleviated by overrating the DC-link capacitor, however this would have physical, financial, and performance-based implications to the system. The DR is a commercially used LVFRT technique and has good performance and can meet grid code expectations. However, the main drawback to this technique is the dissipation of heat and thermal limitations (otherwise, resulting in stresses to the DC-link). In this simulation study, the setpoint of 1.2 pu has been used throughout to include a safety margin as to prevent activation of the DR during wind variations which are common in steady state operation. However, in AC networks with lower SCRs, smaller disturbances cause larger voltage variation and might require higher levels of activation. Albeit increasing technology maturity, SMES has the highest cost, largest physical size, and requires specialist maintenance. SCES has the potential to replace the DR due to the presented high flexibility and controllability, however, higher weight and

**Table 5** Merits and demerits of LVFRT techniques.

| Technique | Merits | Demerits |
|---|---|---|
| Coordinated control (CC) | Low cost<br>No Hardware requirements | Electrical stresses (DC-Link)<br>Mechanical stresses (PMSG) |
| Dumping resistor (DR) | Low complexity<br>Good Performance<br>Low mechanical stress | Heat management<br>Real power overshoots on fault recovery |
| Superconductive magnetic energy storage (SMES) | Good performance | Specialist maintenance requirements<br>High cost<br>Complex hardware requirements<br>Physical weight and dimensions |
| Supercapacitor energy storage systems (SCES) | Superior performance<br>Acceptable weight and size | High self-discharge<br>Complex hardware requirements |

size are still the major challenges. Currently, with all factors taken into consideration, cost and physical limitations are dominating factors of LVFRT technique selection, whist the higher requirement on grid management may inspire the applications of energy storage based techniques in the future.

## 7. Conclusions

In this paper, four low voltage fault ride through (LVFRT) techniques, namely, coordinated control (CC), dumping resistor (DR), superconductive magnetic energy storage (SMES), and supercapacitor energy storage systems (SCES), were presented and investigated to enhance the performance of wind energy conversion systems (WECS). General design has been introduced, and the performance and features have been comprehensively assessed by time-based simulations and critical performance metrics. Although mitigating hardware requirements, the CC is the least effective, and not suitable for LVFRT due to grid code compliance issues and the high level of DC-link voltage during faults. The DR, which has been widely used in industry, was proved to be an effective method of LVFRT; however, concerns arise with the dependence on cooling and overheating due to spurious operation from poorly defined operating set-points could result in a system failure. Such a risk could be reduced by energy storage system (ESS) based methods, which have improved heat management ability and fault energy controllability. Although the simulation results show good LVFRT performance, the high levels of practical complexity and capital costs make SMES currently relatively unrealistic for integration at the wind turbine level. From a simulation perspective, the SCES can offer desirable performance and attractive benefits with flexible use of stored energy cells. Although the practical complexities are lower than SMES, SCES is still commercially immature for such turbine level applications, which is reflected in the capital costs and practical engineering challenges for integration at wind turbine level. Nevertheless, energy storage systems might be suitable for secure renewable system construction.

## Declaration of Competing Interest

The authors declare that they have no known competing financial interests or personal relationships that could have appeared to influence the work reported in this paper.

## References


[1] WWEA, Global Wind Installation, Wind Energy International, 2021. Available from: <https://wwindea.org/worldwide-wind-capacity-reaches-744-gigawatts/> (accessed Dec. 16, 2021).

[2] IEA, Net Zero by 2050: a roadmap for the global energy sector, 2021. Available from: <https://www.iea.org/events/net-zero-by-2050-a-roadmap-for-the-global-energy-system> (accessed Dec. 16, 2021).

[3] S.D. Ahmed, F.S.M. Al-Ismail, M.d. Shafiullah, F.A. Al-Sulaiman, I.M. El-Amin, Grid integration challenges of wind energy: a review, IEEE Access 8 (2020) 10857–10878.

[4] S.W. Ali, M. Sadiq, Y. Terriche, S.A.R. Naqvi, L.Q.N. Hoang, M.U. Mutarraf, M.A. Hassan, G. Yang, C.-L. Su, J.M. Guerrero, Offshore wind farm-grid integration: a review on infrastructure, challenges, and grid solutions, IEEE Access 9 (2021) 102811–102827.

[5] National Grid ESO, System operability framework: impact of declining short circuit level, 2018.

[6] O.P. Mahela, N. Gupta, M. Khosravy, N. Patel, Comprehensive overview of low voltage ride through methods of grid integrated wind generator, IEEE Access 7 (2019) 99299–99326, https://doi.org/10.1109/ACCESS.2019.2930413.

[7] Vestas Wind Systems A/S, V236-15.0 MW ™, 2021.

[8] GE Renewable Energy, Haliade-X offshore wind turbine, 2022. Available from: <https://www.ge.com/renewableenergy/wind-energy/offshore-wind/haliade-x-offshore-turbine> (accessed Mar. 07, 2022).

[9] Siemens Gamesa, The SG 14-236 DD: powering change, 2021.

[10] Siemens Gamesa, Onshire expertise your trusted partner. Available from: <https://www.siemensgamesa.com/en-int/products-and-services/onshore> (accessed Mar. 07, 2022).

[11] Y.-L. Hu, Y.-K. Wu, C.-K. Chen, C.-H. Wang, W.-T. Chen, L.-I. Cho, A review of the low-voltage ride-through capability of wind power generators, Energy Procedia 141 (2017) 378–382.

[12] A.M. Rauf, V. Khadkikar, M.S. El Moursi, A new fault ride-through (FRT) topology for induction generator based wind energy conversion systems, IEEE Trans. Power Delivery 34 (3) (2019) 1129–1137, https://doi.org/10.1109/TPWRD.2019.2894378.

[13] H. Xu, Y. Zhang, Z. Li, R. Zhao, J. Hu, Reactive current constraints and coordinated control of dfig's rsc and gsc during asymmetric grid condition, IEEE Access 8 (2020) 184339–184349, https://doi.org/10.1109/ACCESS.2020.3029227.

[14] J.F.C. and R.F.C. Watson, R., and Watson, J.F. Conroy and R., Low-voltage ride-through of a full converter wind turbine with permanent magnet generator, IET Renewable Power Generation 3 (1) (2007) 182–189, doi: 10.1049/iet-rpg

[15] R.A. Ibrahim, M.S. Hamad, Y.G. Dessouky, B.W. Williams, A review on recent low voltage ride-through solutions for PMSG wind turbine, in: SPEEDAM 2012 - 21st International Symposium on Power Electronics, Electrical Drives, Automation and Motion, 2012, pp. 265–270, doi: 10.1109/SPEEDAM.2012.6264594.

[16] A. Moawwad, M.S. el Moursi, W. Xiao, Advanced fault ride-through management scheme for VSC-HVDC connecting offshore wind farms, IEEE Trans. Power Syst. 31 (6) (2016) 4923–4934, https://doi.org/10.1109/TPWRS.2016.2535389.

[17] C. Kim, W. Kim, Enhanced low-voltage ride-through coordinated control for PMSG wind turbines and energy storage systems considering pitch and inertia response, IEEE Access 8 (2020) 212557–212567, https://doi.org/10.1109/ACCESS.2020.3040905.

[18] X.-Y. Xiao, R.-H. Yang, X.-Y. Chen, Z.-X. Zheng, C.-S. Li, Enhancing fault ride-through capability of DFIG with modified SMES-FCL and RSC control, IET Gener. Transm. Distrib. 12 (1) (2018) 258–266, https://doi.org/10.1049/iet-gtd.2016.2136.

[19] Y. Ma, L. Tao, X. Zhou, X. Shi, Analysis and control of fault ride-through capability improvement for wind energy conversion system using linear active disturbance rejection control with correction link, IEEE Access 8 (2020) 73816–73827, https://doi.org/10.1109/ACCESS.2020.2987103.

[20] X. Sun, C. Shao, Y. Wu, D. Yang, N. Yang, Y. Li, Study on the brake resistor and energy consuming brake process of hybrid electric vehicle, in: Electrical Systems for Aircraft, Railway and Ship Propulsion, ESARS, vol. 2015-May, 2015, pp. 5–10, doi: 10.1109/ESARS.2015.7101450.

[21] B. Wu, Y. Lang, N. Zargari, S. Kouro, Power converters in wind energy conversion systems, in: Power Conversion and Control of Wind Energy Systems, 2011, pp. 87–152, doi: 10.1002/9781118029008.ch4.

[22] J. Dai, D. Xu, B. Wu, N.R. Zargari, Unified DC-link current control for low-voltage ride-through in current-source-converter-based wind energy conversion systems, IEEE Trans.

Power Electron. 26 (1) (2011) 288–297, https://doi.org/10.1109/TPEL.2010.2059377.
[23] G.P. Adam, K.H. Ahmed, S.J. Finney, B.W. Williams, AC fault ride-through capability of a VSC-HVDC transmission systems, in: 2010 IEEE Energy Conversion Congress and Exposition, ECCE 2010 - Proceedings, 2010, pp. 3739–3745, doi: 10.1109/ECCE.2010.5617786.
[24] R. Basak, G. Bhuvaneswari, R.R. Pillai, Low-voltage ride-through of a synchronous generator-based variable speed grid-interfaced wind energy conversion system, IEEE Trans. Ind. Appl. 56 (1) (2020) 752–762, https://doi.org/10.1109/TIA.2019.2946125.
[25] S.D. Ahmed, F.S.M. Al-Ismail, M.d. Shafiullah, F.A. Al-Sulaiman, I.M. El-Amin, Grid integration challenges of wind energy: a review, IEEE Access 8 (2020) 10857–10878, https://doi.org/10.1109/ACCESS.2020.2964896.
[26] F. Islam, A. Al-Durra, S.M. Muyeen, Smoothing of wind farm output by prediction and supervisory-control-unit- based FESS, IEEE Trans. Sustainable Energy 4 (4) (2013) 925–933, https://doi.org/10.1109/TSTE.2013.2256944.
[27] S.-T. Kim, B.-K. Kang, S.-H. Bae, J.-W. Park, Application of SMES and grid code compliance to wind/photovoltaic generation system, IEEE Trans. Appl. Supercond. 23 (3) (2012) 5000804, https://doi.org/10.1109/tasc.2012.2232962.
[28] C. Huang, X.Y. Xiao, Z. Zheng, Y. Wang, Cooperative control of SFCL and SMES for protecting PMSG-based WTGs under grid faults, IEEE Trans. Appl. Superconduct. 29 (2) (2019), doi: 10.1109/TASC.2019.2891908.
[29] H.S. Salama, I. Vokony, Voltage and Frequency Control of Balanced / Unbalanced Distribution System Using the SMES System in the Presence of Wind Energy, 2021, pp. 205–224
[30] C.K. Das, O. Bass, G. Kothapalli, T.S. Mahmoud, D. Habibi, Overview of energy storage systems in distribution networks: Placement, sizing, operation, and power quality, Renew. Sustain. Energy Rev. 91 (November 2016) (2018) 1205–1230, doi: 10.1016/j.rser.2018.03.068.
[31] C. Abbey, G. Joos, Supercapacitor energy storage for wind energy applications, IEEE Trans. Ind. Appl. 43 (3) (2007) 769–776, https://doi.org/10.1109/TIA.2007.895768.
[32] Siegfried Heier, Grid Integration of Wind Energy Conversion Systems, John Wiley & Sons Ltd, 1998, ISBN 0-471-97143-X. doi: 10.1109/63.704150.
[33] M.I. Mosaad, Model reference adaptive control of STATCOM for grid integration of wind energy systems, IET Electr. Power Appl. 12 (5) (2018) 605–613, https://doi.org/10.1049/iet-epa.2017.0662.
[34] S. Mishra, S. Shukla, N. Verma, R. Ritu, Comprehensive review on maximum power point tracking techniques: wind energy, in: International Conference Communication, Control and Intelligent Systems, CCIS 2015, 2016, pp. 464–469, doi: 10.1109/CCIntelS.2015.7437961.
[35] B. Wu, Y. Lang, N. Zargari, S. Kouro, Variable-speed wind energy systems with synchronous generators, in: Power Conversion and Control of Wind Energy Systems, 2011, pp. 275–316, doi: 10.1002/9781118029008.ch9.
[36] B. Wu, M. Narimani, High-power converters and AC drives: second edition, in: High-Power Converters and AC Drives: Second Edition, 2016, pp. 1–451, doi: 10.1002/9781119156079.
[37] E. Hamatwi, I.E. Davidson, M.N. Gitau, G.P. Adam, Modeling and control of voltage source converters for grid integration of a wind turbine system, in: IEEE PES PowerAfrica Conference, PowerAfrica 2016, 2016, pp. 98–106, doi: 10.1109/PowerAfrica.2016.7556579.
[38] P. Rodríguez, J. Pou, J. Bergas, J.I. Candela, R.P. Burgos, D. Boroyevich, Erratum: 'Decoupled double synchronous reference frame PLL for power converters control' (IEEE Transactions of Power Electronics), IEEE Trans. Power Electron. 22 (3) (2007) 1078, https://doi.org/10.1109/TPEL.2007.894351.
[39] European Network of Transmission System Operators for Electricity (ENTSO-E), Requirements for grid connection applicable to all generators, *ENTSOE Standards*, no. October, 2013, p. 86.
[40] D.B.W. Abeywardana, B. Hredzak, V.G. Agelidis, G.D. Demetriades, Supercapacitor sizing method for energy-controlled filter-based hybrid energy storage systems, IEEE Trans. Power Electron. 32 (2) (2017) 1626–1637, https://doi.org/10.1109/TPEL.2016.2552198.
[41] C. Wu, S. Gao, Y. Liu, H. Han, S. Jiang, Wind power smoothing with energy storage system: a stochastic model predictive control approach, IEEE Access 9 (2021) 37534–37541, https://doi.org/10.1109/ACCESS.2021.3063740.
[42] S. Sabihuddin, A.E. Kiprakis, M. Mueller, A numerical and graphical review of energy storage technologies, Energies 8 (1) (2015) 172–216, https://doi.org/10.3390/en8010172.
[43] H.A. Behabtu, M. Messagie, T. Coosemans, M. Berecibar, K. Anlay Fante, A.A. Kebede, J.V. Mierlo, A review of energy storage technologies' application potentials in renewable energy sources grid integration, Sustainability (Switzerland) 12 (24) (2020) 10511, https://doi.org/10.3390/su122410511.
[44] S. Wang, A.M. Massoud, B.W. Williams, A T-type modular multilevel converter, IEEE J. Emerg. Selected Topics Power Electron. 9 (1) (2021) 843–857, https://doi.org/10.1109/JESTPE.2019.2953007.
[45] Q. Xie, Z. Zheng, C. Huang, T. Dai, Coordinated fault ride through method for PMSG-based wind turbine using SFCL and modified control strategy, IEEE Trans. Appl. Supercond. 31 (8) (2021) 1–5, https://doi.org/10.1109/tasc.2021.3103730.
[46] SECOM power, Low voltage Braking Chopper CHT, secompower.com. Available from: <https://www.secompower.com/en/braking-chopper-cht/> (accessed Mar. 11, 2022).
[47] TT Electronics, WDBR5-150RKT Through Hole Thick Film Resistor. Newark.com. Available from: <https://www.newark.com/tt-electronics-welwyn/wdbr5-150rkt/through-hole-thick-film-resistor/dp/71P4644?ost=wdbr5-150rkt> (accessed Mar. 11, 2022).
[48] TE Connectivity, TE Connectivity Passive Product TE2500B100RJ, Digikey.com. Available from: <https://www.digikey.co.uk/product-detail/en/te-connectivity-passive-product/TE2500B100RJ/A121354-ND/2367863> (accessed Mar. 11, 2021).
[49] Infineon, FZ1600R17HP4B2BOSA2, IGBT, 1.7KV, 1.6KA, 10.5KW, Newark.com. Available from: <https://www.newark.com/infineon/fz1600r17hp4b2bosa2/igbt-module-1-7kv-1-6ka-10-5kw/dp/38AJ3608?ost=fz1600r17hp4_b2&autoc=fz1600r17hp4b2> (accessed Mar. 11, 2022).
[50] Maxwell Technologies, 2.7v 100f ULTRACAPACITOR CELL BCAP0100 P270 S07, Available from: <https://maxwell.com/wp-content/uploads/2021/08/2.7V-100F_ds_3001959-EN.4_20200908.pdf> (accessed Mar. 11, 2022).
[51] Eaton Bussmann, XLM-62R1137A-R Supercapacitor, Module, 130 F, 62.1 V, Threaded Stud, XLM Series, Newark.com. Available from: <https://www.newark.com/eaton-bussmann/xlm-62r1137a-r/supercapacitor-130f-62-1v/dp/84AC4632?st=super+capacitors> (accessed Mar. 11, 2022).
[52] Bel Signal Transformer, CH / CL Series Filter Chokes - Single and Dual Windings, belfuse.com. 2019. Available from: <https://belfuse.com/resources/datasheets/signaltransformer/ds-st-sc-series.pdf> (accessed Mar. 11, 2022).